Geomorphology 486 (2025) 109884

Contents lists available at ScienceDirect

Geomorphology

journal homepage: www.journals.elsevier.com/geomorphology

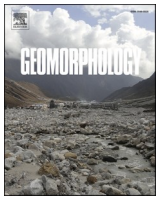

Stratigraphy, evolution and morphology of a sand-rich shoreface

A.N. Green [a,b,c,*], J.A.G. Cooper [c,b], H.L. Draycott [a,d], C. Loureiro [e,a]

[a] Geological Sciences, University of KwaZulu-Natal, Private Bag X54001, Durban, South Africa
[b] School of Geography and Environmental Science, Ulster University, Cromore Road, Coleraine, Northern Ireland BT52 1SA, United Kingdom
[c] South African Institute for Aquatic Biodiversity, Makhanda 6139, South Africa
[d] Fugro Survey (Pty) Ltd, 1 Waterhouse Pl, Century City, Cape Town 7441, South Africa
[e] Centro de Investigação Marinha e Ambiental (CIMA/ARNET), Universidade do Algarve, Campus de Gambelas, 8005-139 Faro, Portugal

ARTICLE INFO

Keywords:
Shoreface
Geological control
Mozambique shelf
Seismic stratigraphy
Morphodynamic state

ABSTRACT

Shoreface morphology and stratigraphic evolution are poorly documented along most of the world's coasts yet are acknowledged to be important influences on shoreline behaviour during changing sea levels. A wide, low gradient, wave-dominated shoreface characterises the area off Xai-Xai in southern Mozambique. It is developed on a Holocene wave ravinement surface cut into deltaic sands punctuated by lithified aeolianite ridges. The 2 km-wide mobile shoreface sand body extends to −23 m depth and averages 10 m in thickness. The modern shoreface bathymetry mimics the underlying wave ravinement surface and this, in turn, is influenced by the presence of aeolianite ridges that create a pronounced break in slope that defines the base of the modern shoreface. The aeolianite influences the wave ravinement profile from which the modern bathymetry is inherited. Comparison with theoretical equilibrium shoreface profile models reveals contrasting shoreface morphodynamic state conditions, dependent upon the model chosen. Based on the model better suited for the lower shoreface. These results emphasize the widely acknowledged but still poorly understood role of geologic inheritance on shoreface morphodynamics and geomorphological evolution, even in sand-rich environments.

1. Introduction

Understanding the evolution, morphology and multi-decadal morphodynamic behaviour of the shoreface remains a challenge because of a relative paucity of observations (Hamon-Kerivel et al., 2020, 2023). Yet, because of its dynamic links to the beach and dune environments, the shoreface exerts a major influence on future shoreline change during sea-level change (Cowell and Kinsela, 2018). Further studies across a wider of a range of shorefaces are required to enhance understanding of their evolution and role in coastal behaviour (e.g. Hamon-Kerivel et al., 2023; Anthony and Aagaard, 2020). As information of shoreface morphology is often lacking, theoretical shoreface equilibrium profiles are often used in shoreline evolution models. These profiles are determined by equations related primarily to the median grain size of shoreface surface sediments (Dean, 1991; Ortiz and Ashton, 2016). In predicting future shoreline behaviour, it is then usually assumed that the shoreface morphology is time-invariant and that it translates landward and upward as sea level rises at the same rate as the shoreline retreat, as proposed in the widely used Bruun Rule (Schwartz, 1967).

There are many objections to this approach, including the observation that grain size cannot be definitively linked to profile slope (Pilkey et al., 1993), and that shorefaces often operate at different temporal scales to the shoreline, giving rise to the potential for shoreface-shoreline decoupling during rapid sea-level rise (Cooper et al., 2018). In addition, recent reviews have shown that active shorefaces exhibit wide variability in morphology (Hamon-Kerivel et al., 2020; Anthony and Aagaard, 2020). The reasons for these variations are not well understood, but Thieler et al. (1995) point out the role of underlying geology in creating accommodation space for shorefaces to exist. Hamon-Kerivel et al. (2020) posit a link between sediment supply and shoreface morphology, with concavity associated with sediment scarcity, and convexity and associated shoreface-connected ridges reflecting increasing degrees of sediment abundance.

The underlying geological influences such as subsurface lithology and morphology, together with sea-level change and inherited sediment characteristics are not well understood, with few studies relating the stratigraphic evolution of the shoreface to the contemporary morphology and morphodynamics of the modern shoreface. Fire Island on the US Atlantic coast remains one of the few well-documented shorefaces from around the world; its temporal evolution and

* Corresponding author at: Geological Sciences, University of KwaZulu-Natal, Private Bag X54001, Durban, South Africa.
E-mail address: greena1@ukzn.ac.za (A.N. Green).

https://doi.org/10.1016/j.geomorph.2025.109884
Received 23 October 2024; Received in revised form 9 June 2025; Accepted 11 June 2025
Available online 14 June 2025

dynamics, as expressed in shoreline-shoreface sediment exchanges, are well understood (Schwab et al., 2013), and in part relate to the underlying geological framework (Hapke et al., 2010).

The aim in this paper is to investigate the geomorphological and stratigraphic evolution of the shoreface from the wave-dominated, high sediment supply southern Mozambique coastline. Such shorefaces are typical of the southeastern coast of Africa; they have a thickly developed sandy prism punctuated by prominent structural controls in the form of aeolianite ridges (Green et al., 2012; Dyer et al., 2021). We examine the stratigraphic development of the shoreface and interpret its development in the context of underlying geological influences (subsurface lithology and morphology), sea-level change and long-term sediment supply. In so doing, we further explore the currently poorly documented role of these factors on shoreface morphology and morphodynamic behaviour.

2. Regional setting

The study area is near Xai-Xai, on the innermost portions of the Limpopo continental shelf of southern Mozambique (Fig. 1). The area is within the Delagoa Bight, a ~ 400 km long WSW-ENE-oriented structural offset marked by a progressive northward widening of the continental shelf and seaward displacement of the shelf break (Dyer et al., 2021). The shelf is narrowest in the south (< 15 km) and widens seawards to Ponta Zavora. It then narrows to the north and assumes an ESE-WNW coastal orientation (Fig. 1). The shelf is characterised by a thick succession of mid Pleistocene deposits (Wenau et al., 2020), mantled by late Pleistocene to Holocene deltaic and aeolianite sequences (Dyer et al., 2021) (Fig. 2). Previous seismic reflection and multibeam bathymetric data from the mid to inner shelf regions revealed thick pro-delta muddy deposits that abut laterally extensive, coast-parallel aeolianites to seaward (Dyer et al., 2021).

The adjoining coastal plain comprises Neogene to Holocene coast-parallel linear dunes (Armitage et al., 2006; Botha and Porat, 2007), with active transgressive dune systems in its seaward margin (Miguel and Castro, 2018; Miguel et al., 2019). These mantle and abut raised aeolianites and beachrocks along the coastline (Miguel et al., 2019). Isolated coastal waterbodies exist north of the Limpopo River and represent impoundment of the water table behind the main coastal barrier system (Miguel et al., 2019).

The southern Mozambican coastline is considered a moderate to high-energy setting with average deep water wave heights of 1.5 m (Cooper and Pilkey, 2002) and a mesotidal spring tidal range of 3 m (Sete et al., 2002). Hoguane et al. (1999) stated that the magnification of the tides along the Mozambican coast can be attributed to the shelf morphology. The coast is dominated by a south-easterly swell regime and a northeast subordinate swell regime, with the former driving the dominant longshore transport to the north (Hoguane et al., 1999; Preu et al., 2011; Cooper and Green, 2023).

The Delagoa Bight Eddy (Fig. 1), a lee-eddy, formed by the southerly flowing Mozambique Current (Lutjeharms, 2006) forms a counter-clockwise flow that causes fluvial discharges from the Limpopo and subordinate rivers to flow north-eastward (Preu et al., 2011; Schüürman et al., 2019). The contemporary sedimentation on the continental shelf is thus mostly controlled by this north easterly current that flows at velocities of 25–30 cm/s up to 150 m depth (Lamont et al., 2010; Preu et al., 2011).

Rivers are the dominant source of terrigenous sediment input to the area (Flemming, 1981), with most of the sediment received from the Limpopo River (Milliman and Meade, 1983). The smaller Lusuftu,

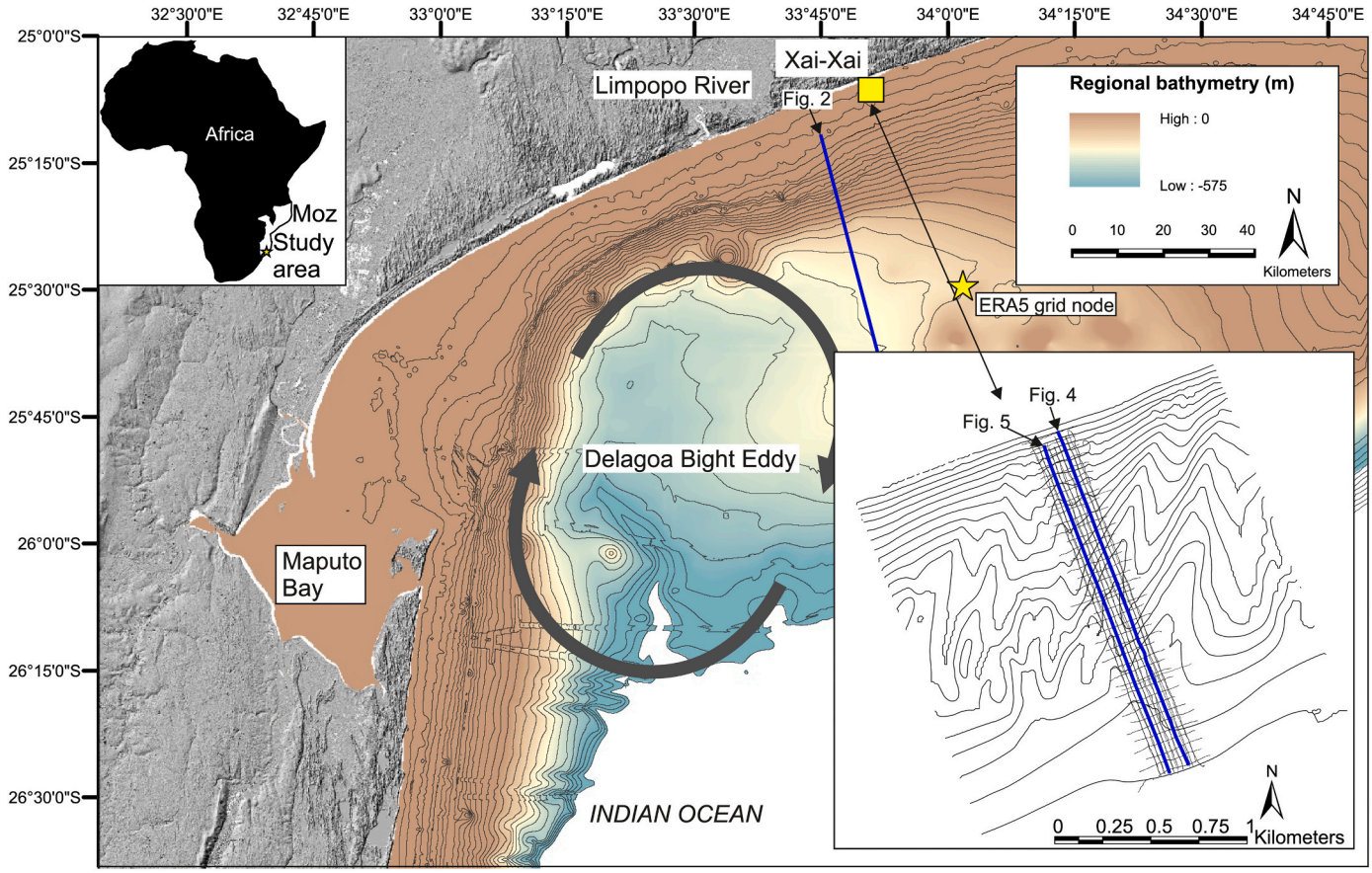

Fig. 1. Location map depicting the general bathymetry of the continental shelf of Delagoa Bight and the location of the Xai-Xai study area. Blue line indicates the seismic profile in Fig. 2 and the yellow star the position of the ERA5 grid node used for obtaining offshore wave data.

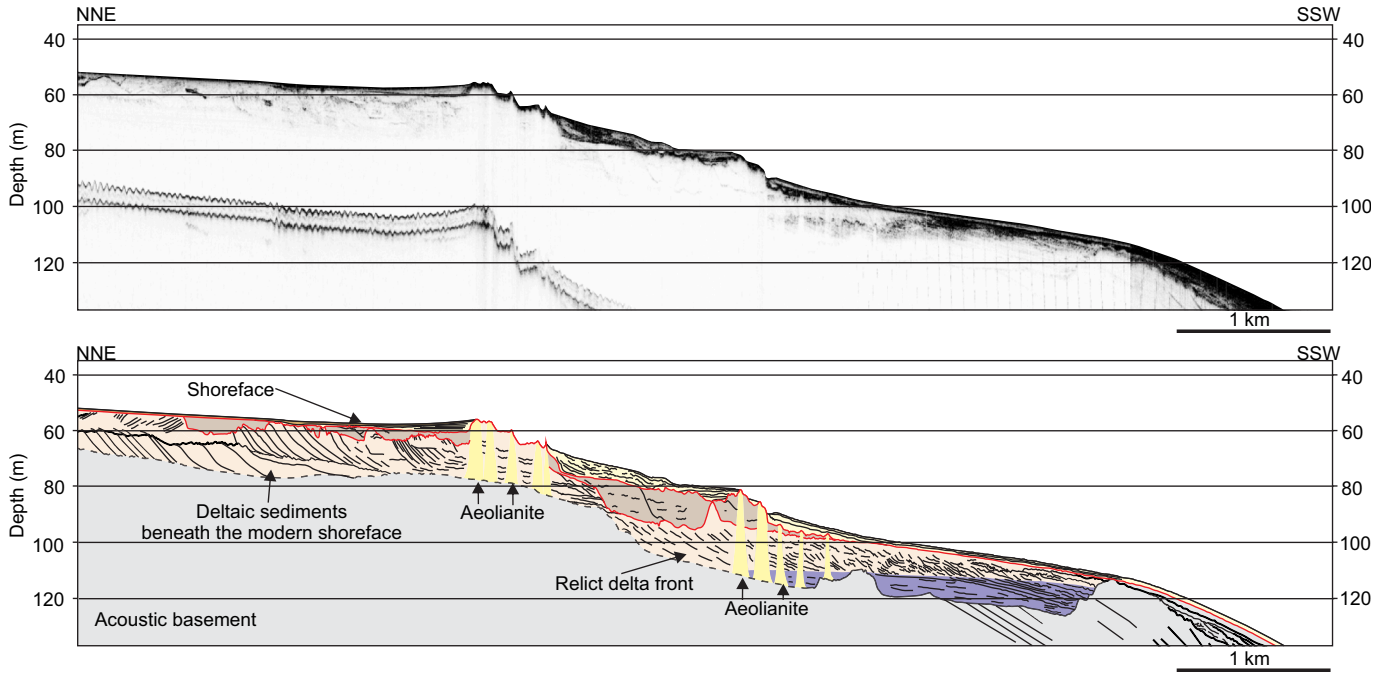

Fig. 2. Seismic reflection profile of the mid to outer shelf, immediately adjacent to the study area. (Adapted from Dyer et al., 2021). There are prominent aeolianites cropping out, the most landward of which dams a thick delta front body that onlaps the aeolianite ridge along its landward edge.

Matola, and Incomati Rivers also provide significant terrigenous materials to the area (Schüürman et al., 2019). Dyer et al. (2021) revealed that an ~20 m thick unit of deltaic sediments have accumulated behind aeolianite barriers on the mid to inner shelf directly offshore Xai-Xai at depths of ~80 m (Fig. 2). The large amount of fluvial-derived sediment transported to the shelf and the overall northward-directed transport regime (Chemane et al., 1997) predispose the shoreface to substantial accumulation of sediment.

3. Methodology

A 4 km^2 section of the lower shoreface was mapped using a combination of geophysical techniques from depths of 5 to 25 m below mean sea level (Fig. 3). Multibeam bathymetry was collected using a 234 kHz RTS2000 system interfaced with a SUBSEA OCTANS motion reference unit. Positioning for all geophysical data was achieved using a Differential Global Navigation Satellite System (DGNSS) with accuracy of 1 m or better. Sound velocity variations were characterised using several sound velocity probe casts performed during the geophysical surveying. Tidal variations in the data were modelled based on a moored Aanderaa WLR7 tide gauge. All data were reduced to mean sea level (MSL) with a resolution of ~1 m and 0.1 m in the horizontal and vertical domains, respectively.

Single-channel seismic reflection data were collected using two separate systems. A lower resolution 200 J boomer system was employed to image the bedrock-sediment interface in the shoreface. The data were collected using an Octopus 360 acquisition system coupled to an 18-element hydrophone array and resolve to ~0.7 m in the vertical domain. The boomer data were co-acquired with higher resolution 3.5 kHz pinger seismic reflection data using a grouping of 4 Massa transducers and recorded on a separate channel with the Octopus 360 system. These data were collected to image the internal architecture of the

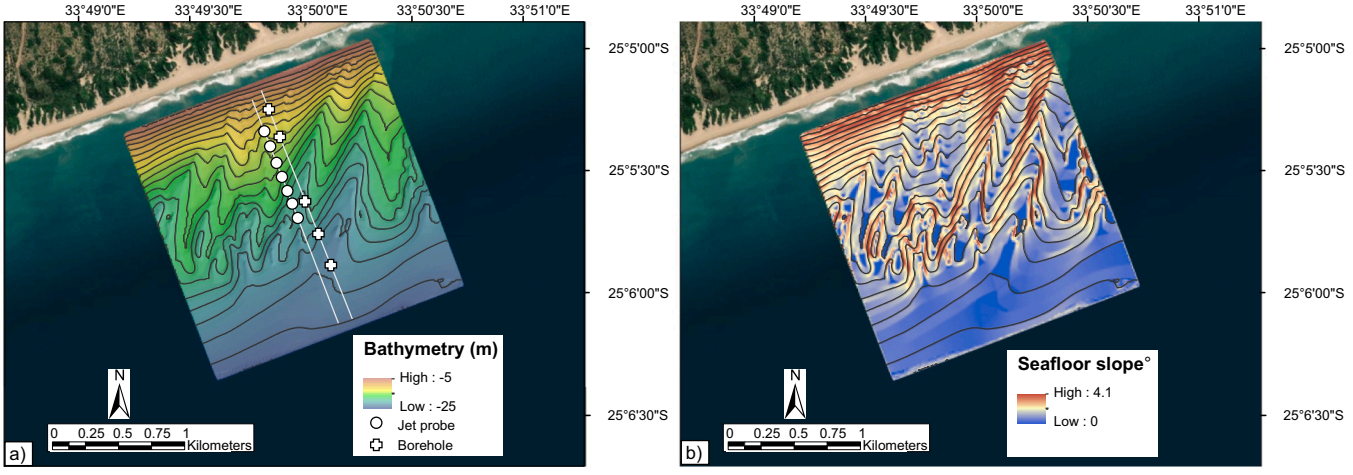

Fig. 3. Seabed bathymetry and slope. a) bathymetric map demonstrating the morphology of several shoreface connected ridges terminating in ~25 m water depths. b) seafloor gradient, depicting the variability in slope and relief of the bathymetry. Coast-oblique shoreface connected ridges form ridge crests with lee faces that dip at up to 2° to the west, with asymmetrical flanks. Depth contours every 1 m from −5 to −25 m.

unconsolidated sediment wedge up to 2 m water depth (~ 20 cm resolution). The data were processed using the Hypack Sub-bottom Profiling software, where both boomer and pinger data were bottom tracked, bandpass and swell filtered. Streamer layback corrections were applied to all boomer data, in addition to the DGNSS antennae offsets. All reflector picking was done in Hypack and referenced to the co-acquired bathymetry surface.

To investigate the lithostratigraphy of the area, five continuous drill cores were retrieved by using a diamond drill and jack up barge. Each core was approximately 45 m long, and all were drilled along the seismic reflection section of interest in a coast-perpendicular fashion (Fig. 3). Cores were split and the material subject to grain size analyses using standard sieving techniques and grain size parameters determined using the logarithmic Folk and Ward (1957) method as implemented in Gradistat (Blott and Pye, 2001). The nature of the surface sediments was assessed by taking the top 5 cm of each core, homogenising these and then analysing their grain size parameters. In addition, water jet probes were deployed parallel to the drill cores and main seismic lines of interest. The water jet probes ranged in length from 13 m to 19 m. The purpose of the drill cores and jet probes was to assess any down dip variability in shoreface composition.

To explore the morphodynamics of the shoreface in the study area, an equilibrium profile modelling approach was used to determine the shoreface morphodynamic state as proposed by Kinsela et al. (2020). This relied on the application of two complementary shoreface equilibrium profile models to determine if the contemporary shoreface is in graded equilibrium, or in overfit or underfit disequilibrium according to the definitions of Daley and Cowell (2012). Following Kinsela et al. (2020), the equilibrium profile model of Dean (1991, hereafter DN91), based on uniform energy dissipation, and the model proposed by Ortiz and Ashton (2016, hereafter OA16), based on the balance of sediment transport following Bowen (1980), were used to determine the theoretical equilibrium shoreface profile for the Xai-Xai coast, and compare it with the average shoreface profile determined from the multibeam bathymetry.

Application of the DN91 equilibrium shoreface profile model was performed using the generalised exponent (m = 2/3) proposed by Dean (1991), with the scaling coefficient ($a = 0.067ws^{0.44}$) defined based on the averaged surface sediment characteristics in the study area, which were determined using the mean grain size of the surface sediments in all the boreholes. Grain size values for the mean and +/− 2 standard deviations were converted into sediment fall velocity (*ws*) according to Soulsby (1997). For the application of the OA16 model, the same sediment fall velocities for mean and +/− 2 standard deviation of the grain size were used, and in addition the characteristic wave height and period were determined as prescribed by Ortiz and Ashton (2016). Offshore significant wave and peak wave period data from the nearest grid node (Fig. 1) of the ERA5 global reanalysis (Hersbach et al., 2020) were used, as ERA5 was found to appropriately represent mean wave conditions in the SW Indian Ocean coast, despite minor overestimation (underestimation) of wave height (period) (Fanti et al., 2023). Deepwater (~280 m water depth) ERA5 wave data were extracted for the period 1979–2021, and then shoaled to 30 m water depth using linear wave theory to obtain a more accurate representation of wave conditions along the shoreface of the study area. To further investigate the influence of variable grain size on theoretical shoreface profiles, the OA16 model was also implemented considering the median value for sand size classes, as defined by Blott and Pye (2001), identified in the cores (very fine sand – 0.094 mm, fine sand – 0.175 mm, medium sand – 0.375 mm, coarse sand 0.750 mm).

In addition to the application of the shoreface equilibrium models described above, the theoretical limits of the shoreface were defined according to Hallermeier (1981), including the determination of the annual depth of closure (*DoC*) based on the yearly 12 h exceedance of significant wave height ($H_{s(30)\ 12h}$) and associated peak period. The inner (d_l) and outer (d_i) limits of the shoal-zone were also defined according to Hallermeier (1981) based on the mean and standard deviation of the shoaled significant wave height. Finally, the morphodynamic depth of closure proposed by Ortiz and Ashton (2016) to determine the surface response timescales across the shoreface was also calculated for the yearly ($MODC_{1yr}$), decadal ($MODC_{10yr}$) and centennial ($MODC_{100yr}$) timescales.

4. Results

4.1. Lower shoreface morphology and sedimentary characteristics

The seafloor of the lower shoreface is dominated by a series of high-relief shoreface-connected ridges (SCRs) (Fig. 3). The ridge crests slope seaward at ≤0.5–1° (Fig. 3b) and extend seaward from the shoreline for approximately 1 km (Fig. 3a). Their crests are aligned coast-obliquely (NNE-SSW) (Fig. 3a) and are spaced 400 m to 600 m apart. The ridge heights are between 3 and 4 m (Fig. 3a), and they are asymmetrical, with a 1.5°-2° slope on the western-facing slopes and gentler gradients on the eastern-facing slopes (Fig. 3b).

For the first ~1 km from the shoreline, the shoreface reflects a steep, linear to concave up profile between −5 m and − 22 m (Fig. 3). In the lower part of the shoreface, seaward of the SCRs, and below 22 m depth, the seabed flattens, with a gentler (0° - 1°) gradient (Fig. 3b). Taking *DoC* or d_l as the upper shoreface depth limits results in identical estimates of ~9.5 m water depth (Table 1), while the lower shoreface depth limit d_i of −32.1 m indicates a considerably deeper theoretical limit for the active shoreface profile than evidenced by the flattening at −22 m. Considering the morphodynamic depth of closure as proposed by Ortiz and Ashton (2016), the depth of −22 m would correspond approximately to the 10 yr MODC, while at the centennial timescale the theoretical limit for the shoreface profile determined exclusively by wave-driven transport across the wave shoaling zone would extent to −29.4 m. The grain size parameters of the surface sediments in the 9 boreholes evidence similar characteristics across the entire shoreface, overwhelmingly composed by medium sand with averaged mean (median) grain size of 0.442 mm (0.278 mm), generally poorly sorted but mostly symmetrical (Table 2).

4.2. Seismic and lithostratigraphy of the shoreface and underlying units

Several sedimentary units and surfaces were identified based on seismic reflection profiles, drill cores and jet probe data (Figs. 1 and 3). These include six main units with five major seismic stratigraphic surfaces (Figs. 4 and 5). The distribution and thickness of the units and underlying shoreface substrate are shown in Fig. 6.

4.2.1. Unit 1

The lowermost unit is composed of indistinct, low to moderate amplitude seaward-dipping reflections (Fig. 4a). Though reflections are largely obscured by acoustic masking of the multiple reflections, there is evidence in the boreholes of a seaward dipping pebbly gravel horizon

Table 1
Theorethical limits for the Xai-Xai shoreface based on Hallermeier (1981) and Ortiz and Ashton (2016).

Parameter	Value (m)
DoC	−9.5
d_l	−9.6
d_i	−32.1
$H_{s(30)\ 12h}$	4.7
$H_{s(30)\ mean}$	1.6
$H_{s(30)\ standard\ deviation}$	0.6
$MODC_{1yr}$	−17.2
$MODC_{10yr}$	−22.5
$MODC_{100yr}$	−29.4

Table 2
Depth and grain size parameters for the surface samples in the boreholes from the shoreface of Xai-Xai.

Borehole	Depth (m MSL)	Mean (μm)	Median (μm)	Sorting (ϕ)	Skewness (ϕ)	D_{16} (ϕ)	D_{50} (ϕ)	D_{84} (ϕ)
3	12.4	454	272	1.99	−0.05	0.15	1.88	2.41
4	14.0	449	289	1.76	0.08	0.13	1.79	2.82
5	18.9	513	302	1.91	−0.07	−0.02	1.73	2.16
6	18.9	451	265	1.92	−0.02	0.11	1.91	2.62
7	19.1	449	269	1.72	0.01	0.12	1.89	2.66
7a	19.3	455	243	2.08	−0.25	0.15	2.04	2.18
8	19.8	436	294	1.97	0.15	0.16	1.76	3.08
9	20.7	446	279	1.76	0.08	0.12	1.84	2.85
10	21.4	344	289	1.99	0.28	0.73	1.79	2.85

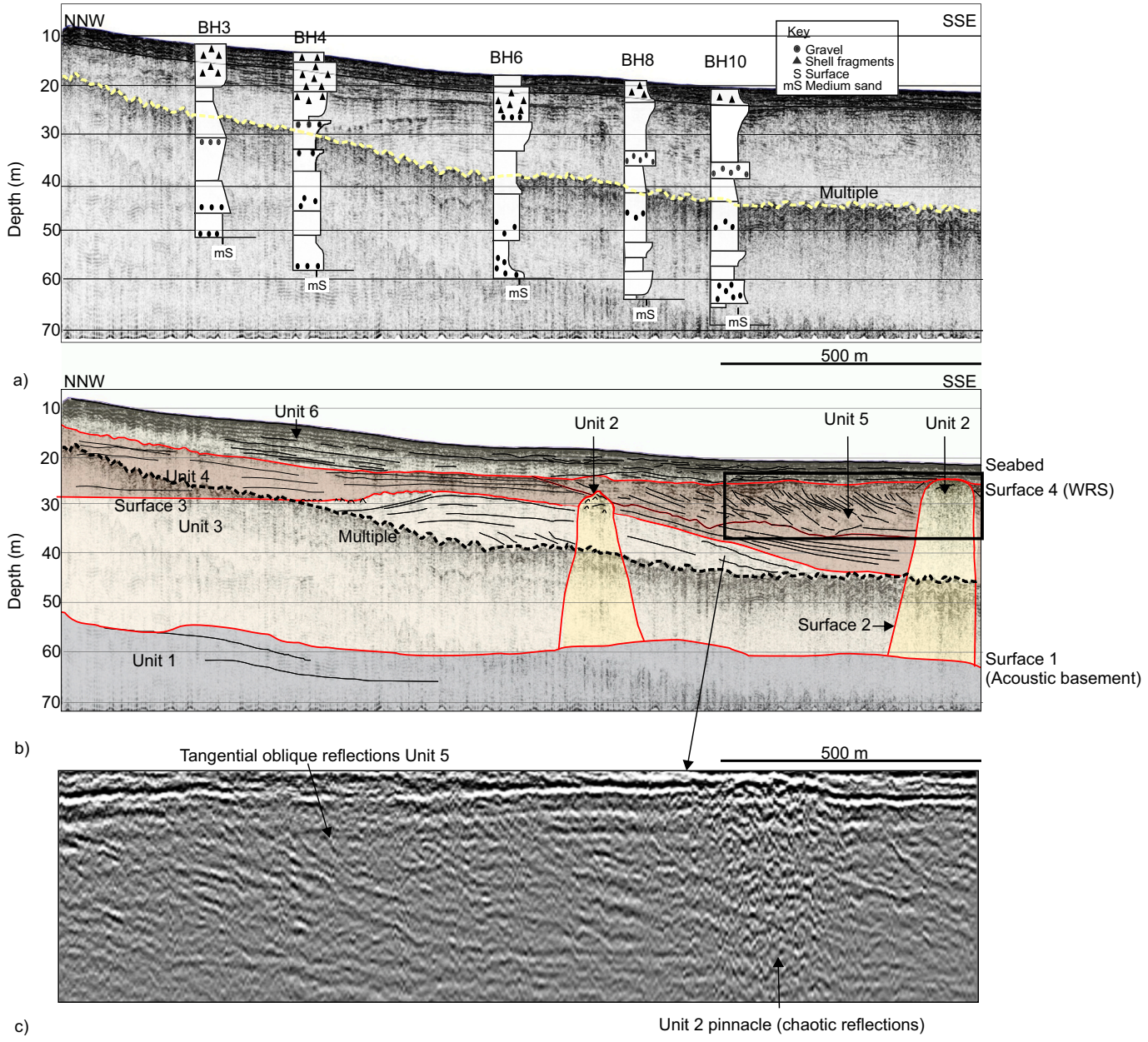

Fig. 4. (a) Uninterpreted NNW-SSE trending boomer seismic reflection profile (for location see Figs. 1 and 3) with boreholes overlain. (b) interpreted seismic stratigraphic units and key stratigraphic surfaces (in red). Note the presence of two pinnacles of Unit 2. Blow up of raw seismic data showing tangential oblique reflections of Unit 5. WRS – wave ravinement surface. Seafloor multiple highlighted in light yellow (top) and black (bottom).

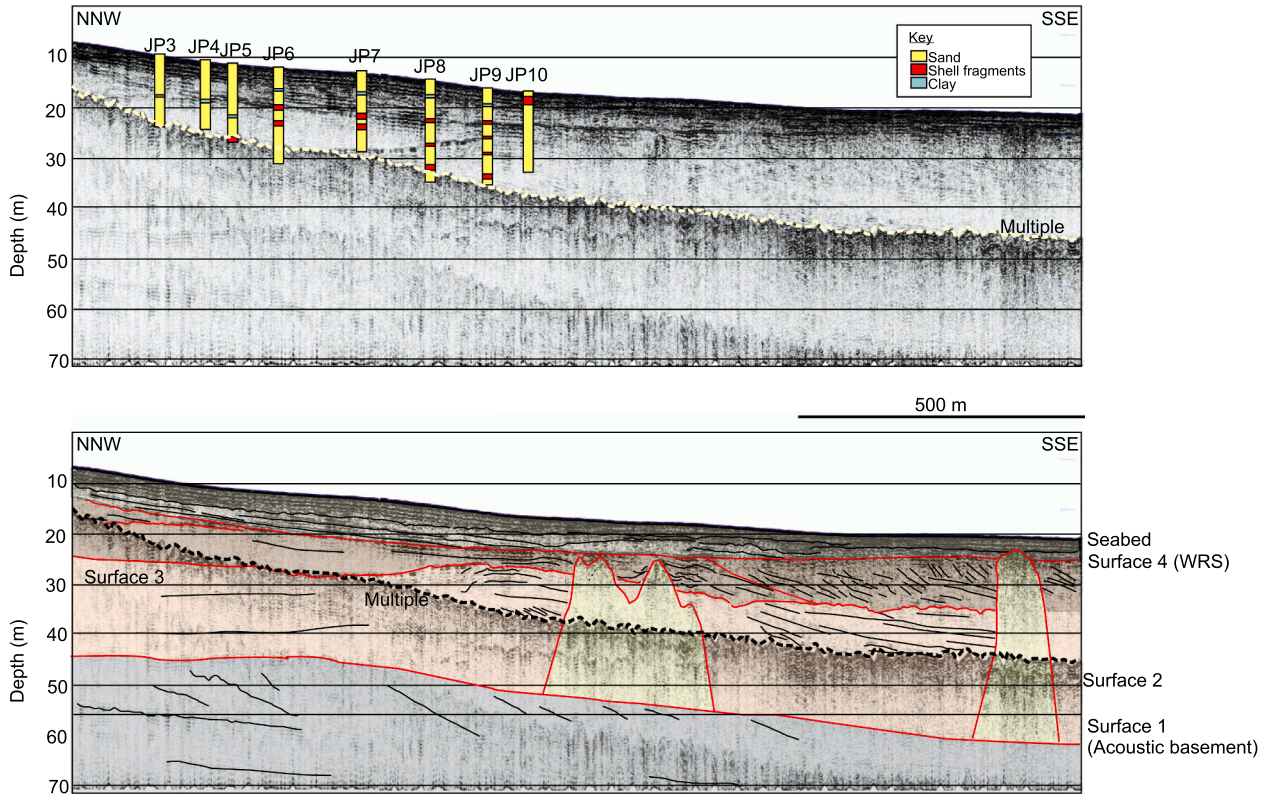

Fig. 5. (a) Uninterpreted NNW-SSE trending boomer seismic reflection profile (for location see Figs. 1 and 3) with jetprobes overlain. (b) interpreted seismic stratigraphic units and key stratigraphic surfaces (in red). Note the presence of two pinnacles of Unit 2. Jet probes (JP) are shown depicting the down dip change in sediment type. WRS – wave ravinement surface. Seafloor multiple highlighted in light yellow (top) and black (bottom).

(Surface 1) that marks the uppermost surface of the unit at depths of 48 m to 68 m below mean sea level (Fig. 4b). Surface 1 reflects an irregular relief horizon with minor NNE-SSW-oriented channels ~1 m deep and up to 70 m-wide (Fig. 6a).

4.2.2. Unit 2

High-relief, acoustically opaque pinnacles with crest elevations from −50 m to −23 m overlie unit 1 (Figs. 4, 5 and 6b). These form several coast-parallel, 35 m-thick pinnacles comprising three main ridges with bases at between −55 m and − 65 m (Fig. 6c). This unit characteristically obscures the acoustic signal and stratigraphy below (Figs. 4 and 5).

4.2.3. Units 3, 4 and 5

Unit 3 reflects a thick accumulation of sediment in the form of a seaward-pinching wedge (Figs. 4 and 5). The mostly sigmoidal-oblique internal reflections dip seaward, with occasional landward-orientated reflections. Their relationship with Surface 1 is not clear due to multiples masking the stratigraphy. Unit 3 is thickest to landward of Unit 2 where it reaches ~40 m in thickness (Fig. 6d). A narrow ≤35 m thick apron of Unit 3 abuts the seaward edge of the most landward ridge of Unit 2. Proximally, the unit comprises a fining upward package of medium to fine sands, with occasional shelly horizons occurring landward (Fig. 4a and Fig. 5).

Unit 4 comprises a series of moderate amplitude, tangential oblique prograding reflections that downlap and onlap Surface 2 and which are in turn truncated by Surface 3, an irregular low to moderate amplitude reflector (Fig. 6e). The internal reflections transition into flat-lying parallel reflections to landward of the Unit 2 pinnacles. The lithological data from the boreholes reveal that this unit comprises a coarsening up sequence of medium to coarse sands, capped by a distinctive layer of pebbly gravel (Fig. 4a). This layer marks the presence of the irregular erosional surface (Surface 3) that separates unit 3 from the overlaying units 4 and 5.

Unit 5 comprises a series of tangential oblique, steeply dipping prograding reflections with minor internal discontinuities. The unit corresponds to a sandy, coarsening upward sediment body (Fig. 4a). Unit 4 and 5 reach a combined thickness of ~22 m and cover the more inshore Unit 2 feature (Fig. 6f). The two units thicken considerably to landward of the deepest Unit 2 ridge. Both Units 4 and 5 are truncated by a gently seaward dipping, concave-up, high-amplitude erosional reflector (Surface 4) (Fig. 6g). The surface is marked by the occurrence of shells and shell fragments and an increase in grain size from fine to coarse sand (Fig. 4a and Fig. 5).

4.2.4. Unit 6

Unit 6 is the shallowest unit, representing the modern mobile shoreface. The unit comprises seaward-dipping, planar to irregular, and sometimes wavy reflections with minor discontinuities evident to a depth of ~22 m. Unit 6 thins seaward, with thicker accumulations of material (≤ 11 m) corresponding to the SCRs observed in the bathymetry (Fig. 3).

4.3. Architecture of major stratigraphic surfaces

The acoustic basement (Surface 1, Fig. 4) is a low relief, gently seaward dipping unconformity that ranges in depth from −50 m to −67 m and on which Unit 2 rests (Fig. 4a). This gentle and uniform slope contrasts with the more variable overlying seismic stratigraphic surfaces and contemporary bathymetry (Fig. 7a).

The high-relief pinnacles of Unit 2 dominate the stratigraphy and contribute to topographic variation in the key overlying stratigraphic surface 4 (Fig. 4a). Surface 4 has a pronounced increase in slope landward of the pinnacles of Unit 2 (Fig. 7b). This inflection point is in turn mirrored in the seabed bathymetry, where the bathymetric inflection

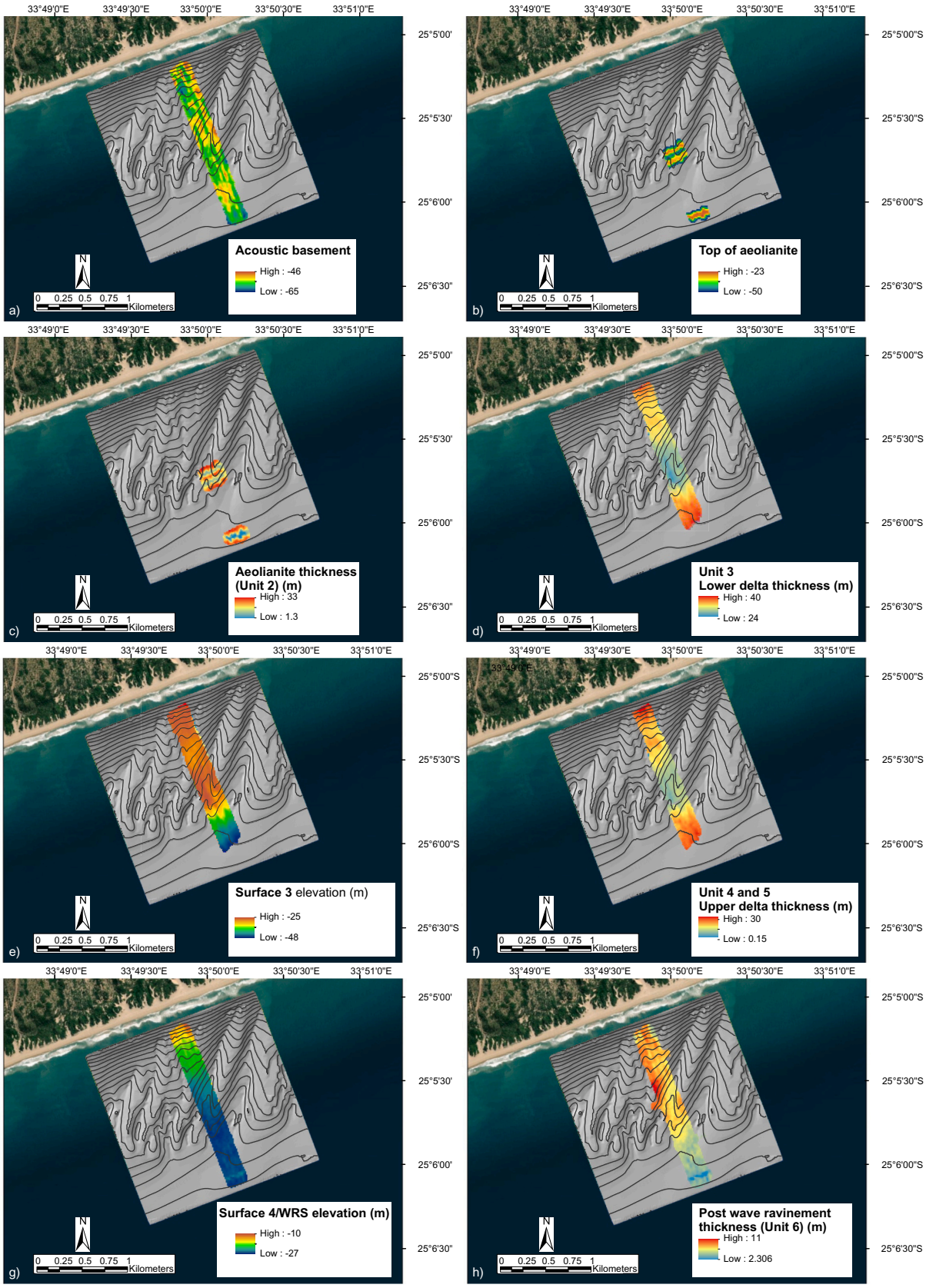

Fig. 6. Depth/structure maps for the stratigraphy. (a) Elevation of acoustic basement, (b) top of aeolianite surface, (c) aeolianite thickness, (d) lower delta thickness, (e) surface 3 elevation, (f) upper delta thickness, (g) elevation of the wave ravinement, (h) post wave ravinement sediment thickness.

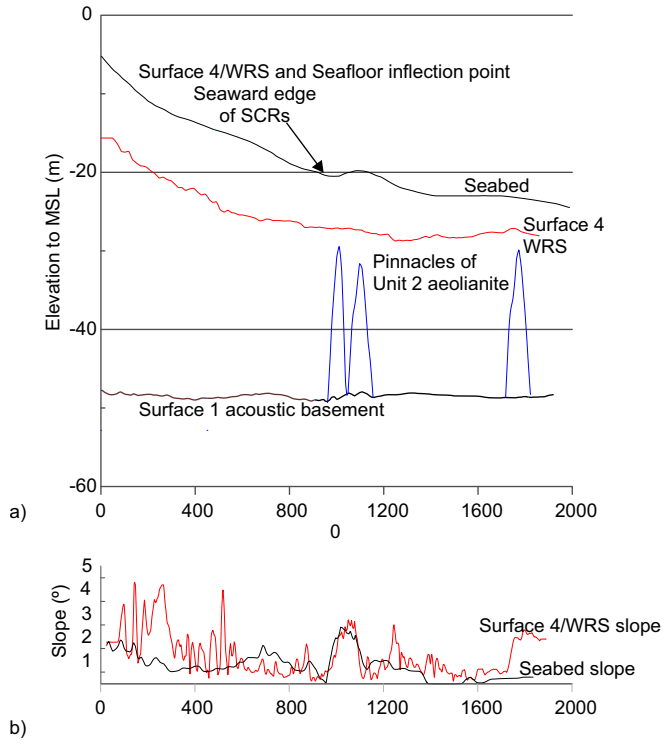

Fig. 7. Cross sections of the major stratigraphic surfaces of the study area: a) major stratigraphic surface elevations; (b) cross sectional variation in slope of surface 4 (red) and the seabed (black), highlighting the distinct similarity in the morphology of surface 4 and the seabed. The inflection point in slope of both the seabed and Surface 4 corresponds with the pinnacles of the underlying unit 2. WRS – wave ravinement surface.

point depicted in Fig. 7b accompanies the increase in the relief of Surface 4. Landward of these pinnacles, Surface 4 rises steeply from −30 m to −15 m, in a concave-up configuration (Fig. 7a), while seaward the gradient of Surface 4 flattens considerably, as does that of the seabed (Fig. 7b).

4.4. Modelled and measured shoreface profiles

The observed averaged shoreface profile was compared to theoretical equilibrium profiles derived according to the sediment and wave conditions in the study area. To determine the characteristic wave height and period required for the OA16 model, wave conditions were weighted based on the contribution to sediment transport as proposed by Ortiz and Ashton (2016) and combined using a bivariate histogram (Fig. 8), with the centre of mass of the distribution corresponding to the morphodynamically significant wave height and period. These were 3.8 m and 12.1 s, respectively. These effective wave conditions are characteristic of a moderate to high-energy wave setting. Combined with mean grain size (average = 0.442 mm, +/− 1 (2) standard deviation 0.044 (0.088) mm) and corresponding sediment fall velocity (average = 0.0587 m/s and +/− 1 (2) standard deviation = 0.0011 (0.0022) m/s) determined from borehole surface sedimentology, the theoretical equilibrium profiles indicate contrasting conditions (Fig. 9). The same approach was implemented with the averaged median grain-size and +/− 1 (2) standard deviation, but the results are not substantially different (as shown in Fig. S1 in the supplementary information).

Following Kinsela et al. (2020), equilibrium profiles determined using the OA16 model were translated to the origin of the surveyed profile seaward of the nearshore bars at −5 m water depth, as the model is based on wave shoaling processes and not appropriate to represent the general slope of the surf zone. Conversely, the DN91 equilibrium profile was not translated, and the origin is set at mean sea level, as this

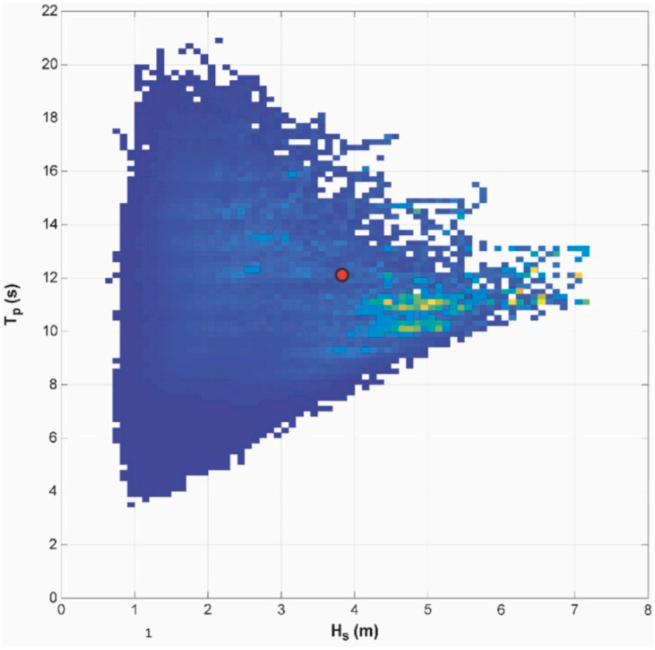

Fig. 8. Weighted wave height and wave period bivariate distribution reflecting the characteristic morphodynamic wave height and wave period for Xai-Xai (red dot).

equilibrium profile model is considered to be representative of the averaged surf zone and upper shoreface profile.

Both modelled equilibrium profiles evidence a concave up profile configuration that is similar to the shoreface bathymetry. According to DN91 the theoretical equilibrium profile is shallower than the observed bathymetric profile of the study area (Fig. 9a) and would be regarded as indicative of disequilibrium underfit in morphodynamic state. Based on the OA16 model, however, the theoretical equilibrium profile is deeper than the observed bathymetric profile, and the shoreface morphodynamic state suggests disequilibrium overfit (Fig. 9b). Even when considering the range of sediment size found in the seabed of the study site, represented by +/− 2 standard deviations of the averaged mean grain size, both theoretical equilibrium profiles still deviate significantly from the observed profile.

As sediment size is often considered the primary control on shoreface equilibrium profile models, the OA16 model was also run for the same wave parameters but using the median value of sediment classes found in the cores of the Xai-Xai shoreface (i.e., very fine sand, fine sand, medium sand, coarse sand). Improved agreement between observed and modelled shoreface equilibrium profile is achieved when the OA16 model is run for fine sand, with significant departures from the observed bathymetry in all other cases (Fig. 9c). Minor deviations between the observed and modelled profile for fine sand occur close to sections of higher bathymetric variability, represented by wider +/− 2 standard deviation bands around the mean observed profile (Fig. 9c).

5. Discussion

5.1. Stratigraphic interpretation

5.1.1. Acoustic basement

Unit 1 is the oldest unit in the study area and constitutes the acoustic basement. Though the presence of gently seaward dipping reflections is visible, most of the unit is obscured by acoustic masking. This unit likely represents the landward continuation of the delta top deposits recognised by Dyer et al. (2021). The age of deposition for the unit is uncertain. The seaward dipping pebbly gravel horizon of Surface 1

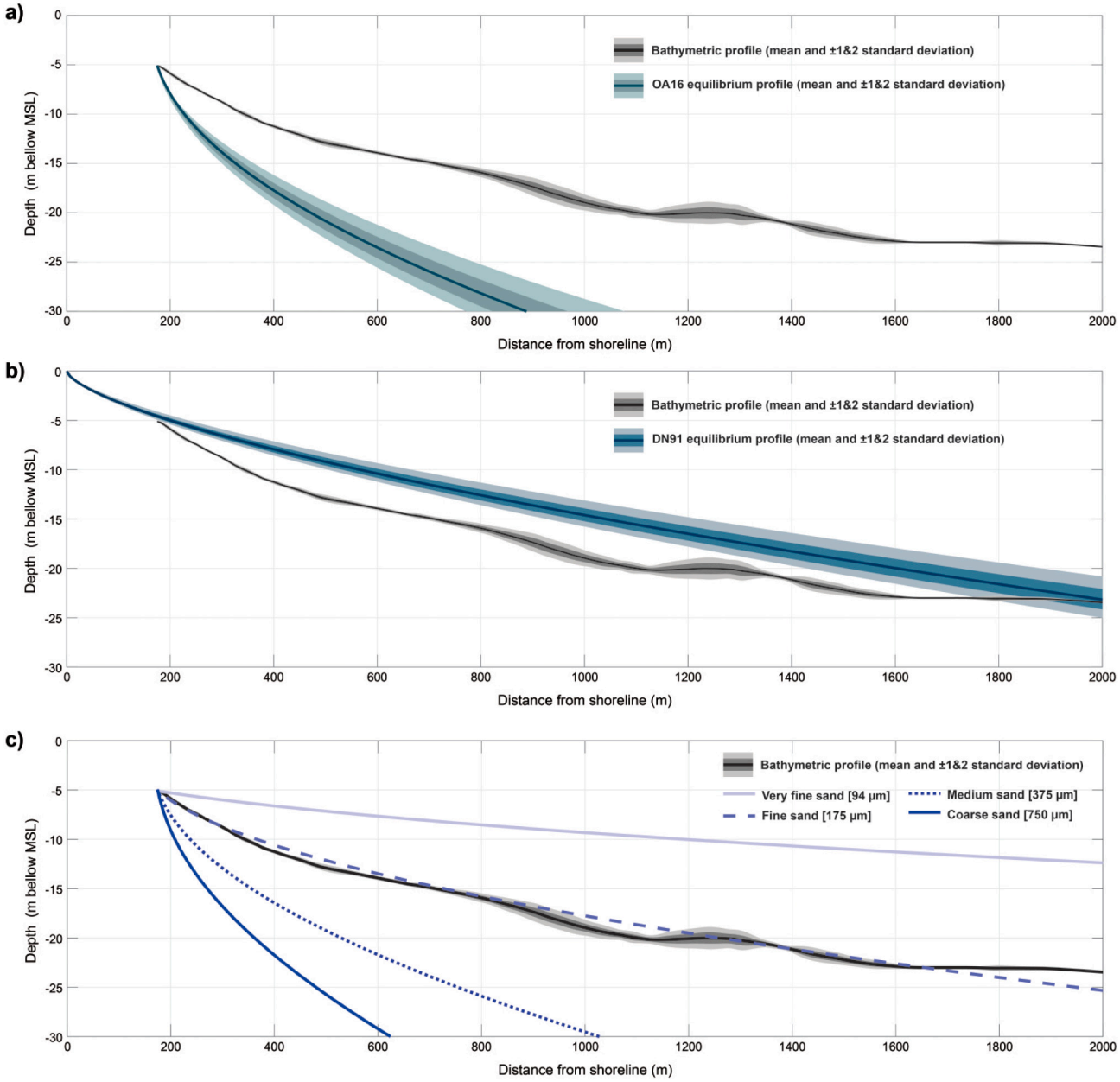

Fig. 9. Equilibrium and observed shoreface profiles for Xai-Xai based on the mean grin size of shoreface surface sediments: a) DN91 equilibrium profile; b) OA16 equilibrium profile; c) additional OA16 equilibrium profiles for the four main sand classes found in the surface sediments of the study area.

indicates a truncation of Unit 1 and likely relates to the erosional surface produced by migrating delta top channels during rising sea levels in the late Pleistocene and early Holocene (Dyer et al., 2021, Fig. 2).

5.1.2. *Aeolianite pinnacles*

The high relief and acoustically opaque nature of the pinnacles of Unit 2 are characteristic of aeolianite ridges observed throughout Maputo Bay (De Lecea et al., 2017), the Limpopo shelf (Wenau et al., 2020; Dyer et al., 2021) and the adjoining coastal plain (Miguel et al., 2019). Despite not being directly sampled in this study, samples of similar aeolianite from the KwaZulu-Natal shelf to the south of the study area reveal them to comprise well-sorted, carbonate-cemented sands (Richardson, 2005), the base of which may occur on unconsolidated sediment due to the variable position of the freshwater phreatic surface at the time of cementation (Bateman et al., 2004). Once submerged, these form the most prominent topographic features of the SE African shelf (Green et al., 2014, Dyer et al., 2021). It is clear that these aeolianite pinnacles exert a primary control on the geometry of all successive major stratigraphic surfaces above them (Fig. 7), such that even the current seafloor morphology is similarly influenced by their position in the subsurface.

5.1.3. *Delta front deposits*

The sigmoidal prograding reflections within Unit 3, together with its mounded geometry and sporadically bi-directionally dipping reflections compare well with the internal geometry of other sandy deltaic bodies preserved in the shelf stratigraphy seaward of the study site (Dyer et al., 2021) and are likely associated with the Limpopo River delta. Similar stratigraphic architectures are reported from sediment bodies on the adjacent South African shelf where the Thukela River also builds a subaqueous delta (Engelbrecht et al., 2020, 2022). Like those examples, the deposits of Unit 3 thicken where they abut aeolianite bodies to seaward, implying strong geological control on their development during delta construction and later rollover phases.

The gently inclined flat-lying and uniformly parallel reflections in the proximal part of Unit 4 transition to oblique tangential reflections where Unit 2 is encountered. These are in turn overlain to seaward by another, package of oblique tangential reflections though without the same landward continuity into flat-lying reflections. Like Unit 3, these are interpreted as delta front deposits, with proximal delta top (flat-lying topsets) preserved in Unit 4, but separated from Unit 5 by the erosion that produced Surface 4.

The entire stack of Unit 3–5 thus represents periods of normal regressive sandy deltaic outbuilding, an interpretation corroborated by the upward-coarsening nature of the lithologies in the overall sediment package (Figs. 4 and 5). The position of the most landward aeolianite pinnacle dictated both the rollover of the Unit 4 delta, and the onlap point of the Unit 5 delta front with the previous Unit 4 delta body. The rollover positions are proximal relative to the modern shoreline, with rollover depths between 27 and 30 m, indicating their deposition during periods of lower than present sea level and high sediment supply. Unit 5's topsets are entirely truncated by Surface 4.

5.1.4. Wave ravinement surface (WRS)

The erosional, high-amplitude Surface 4, revealed in the boreholes by an increased grain size associated with occurrences of shells and shell fragments, corresponds to the Holocene wave ravinement surface. Similar wave ravinement surfaces were documented by Pretorius et al. (2016, 2018) and De Lecea et al. (2017) on the SE African shelf. The overlying sediment is representative of a lower shoreface setting, marked by a seaward tapering wedge of sand that fines upward, indicative of progressive deepening of the shelf environment during landward shoreline migration (e.g. Zecchin, 2007).

Landward of the aeolianite pinnacles the wave ravinement surface profile shows consistent steepening, indicating a change in shoreline trajectory. This was influenced by the presence of a harder substrate as the wave base translated over the mostly sand-dominated deltaic sediment bodies. In contrast, seaward of, and between the aeolianite pinnacles the ravinement profile is uniformly flat. The topsets of Unit 5 were removed by wave ravinement processes, however, the change in trajectory of the erosion surface marks the point where preservation of the underlying deltaic topsets of Unit 4 began.

Steepened trajectories of shoreface erosion can be ascribed to several factors. The primary factor is related to aggradation rates of the shoreface, whereby sediment supply determines the shoreline trajectory (Helland-Hansen and Martinsen, 1996). In such cases, an aggrading shoreface may define the ravinement trajectory by localised steepening and divergence of multiple erosion surfaces during the transgression process (Steel et al., 2000). Alternatively, the gradient over which the shoreline translates can control the accumulation of transgressive materials and in turn allow a divergence of the ravinement profile from the surface being transgressed (Cattaneo and Steel, 2003). Low-gradient settings produce thin shoreface deposits and a low angle ravinement profile that merges up-dip with the transgressed surface. In contrast, high gradient settings (assumed to be coupled to high sediment supply) may also produce steep ravinement profiles and multiple wave ravinement surfaces (Cattaneo and Steel, 2003).

In the case of the Xai-Xai shoreface, only one wave ravinement surface is observed capping the high-sediment-supply deltaic sequences. Though sediment supply has undeniably controlled to some extent the overall shoreface trajectory at Xai-Xai, the sudden steepening of the single wave ravinement profile, associated with the pinnacles of the underlying aeolianites is in contrast with the above models. Pretorius et al. (2016) and Engelbrecht et al. (2022) also recognised a situation where strong geological control by hard aeolianite substrate caused localised steepening of the wave ravinement and a decoupling of the shoreface from the surf zone, resulting in relict shoreface sediments preserved downdip in the offshore zone.

5.2. Sediment supply and geological control

Multiple phases of delta construction, with sediment accumulation of up to 40 m, indicate significant quantities of fluvial sediment input (mainly from the Limpopo River), to the shelf around Xai-Xai, and a high degree of post-ravinement preservation of these materials. This would suggest, in principle, that sediment supply to the Xai-Xai shoreface is so abundant that it would overprint underlying geological controls on shoreface configuration. However, despite this, in the case of Xai-Xai the underlying geological control is manifest in the control on the wave ravinement profile and the subsequent mirroring of the ravinement surface in the contemporary shoreface bathymetry.

Previous work on multiple sites along the USA coast by Ortiz and Ashton (2016) found that modelled equilibrium shoreface profiles were comparatively similar to observed profiles for most locations, except where geological inheritance was strong. Such findings supported the assertion of Dean (1991) that, in the absence of strong geological control, sediment grain size exerts the primary control on equilibrium shoreface slope in wave-dominated coastal settings. Comparing the equilibrium profiles computed for different grain sizes (Fig. 9c), under the characteristic wave energy conditions of Xai-Xai, only the equilibrium profile modelled for fine-sand approximated the observed shoreface profile.

In addition to the role of sediment texture and wave regime in determining the shoreface profile, the presence of underlying geological and stratigraphic features is also a fundamental control on shoreface morphology (Pilkey et al., 1993, Cooper and Pilkey, 2004, Cooper et al., 2018; Kirkpatrick and Green, 2018). Riggs et al.'s (1995) observations from a sediment-rich, wave-dominated transgressive shoreface in North Carolina highlight the presence of submarine headlands whose influence bears comparison to the aeolianites in the study area. Riggs et al. (1995) showed that preservation of the headlands influenced the shoreface profile because they manifest as bathymetric highs, cropping out in the mobile shoreface environment. Consequently, they influence incoming waves and currents and, in turn alter sediment dynamics and shoreface morphology. The crests of buried aeolianites in the Xai-Xai shoreface, which intersect the wave ravinement surface, may similarly be anchoring points for shoreface connected ridges.

However, given the longer timescales involved in development of the broader shoreface configuration, the steeper concave shoreface geometry would be expected to extend beyond the −29.4 m of the 100 yr MODC, if the shoreface profile was exclusively controlled by wave-driven sediment transport throughout the wave shoaling zone.

5.3. Shoreface morphodynamic state

The morphodynamic state of sedimentary shorefaces can be considered according to the potential for sediment exchange and morphological change (Anthony and Aagaard, 2020), with potential implications for coupled shoreface and shoreline response to sea-level rise (Kinsela et al., 2020). Based on the comparison between the theoretical shoreface equilibrium profile and the observed bathymetry, shoreface morphodynamic states can be classified as being in underfit or overfit disequilibrium, or alternatively in graded equilibrium (Daley and Cowell, 2012; Kinsela et al., 2020).

In the case of Xai-Xai, the equilibrium profiles from the DN91 and OA16 models indicate contrasting morphodynamic states, with disequilibrium underfit for DN91 (Fig. 9a), and disequilibrium overfit for OA16 (Fig. 9b). The absence of bathymetric information for the upper shoreface prevents an evaluation of the DN91 model in the surf-zone, for which it is better suited. However, the results from Xai-Xai share similarities with findings for the New South Wales coast presented by Kinsela et al. (2020), where DN91 also evidences poor agreement indicative of underfit across most of the shoreface. Underfit disequilibrium is characterised by positive sediment accommodation, as the shoreface is too deep or too steep to reach equilibrium, despite the

abundant sediment supply. This allows sediment mobilised in the upper shoreface to be transported offshore and sequestered in the lower shoreface (Daley and Cowell, 2012). Therefore, geological control predominates on the upper shoreface while the lower shoreface morphology reflects abundant accommodation and high rates of sediment supply.

In contrast to DN91, the overfit disequilibrium predicted by the OA16 model (Fig. 9b) is indicative of a shallow shoreface with negative accommodation and overfilled with sediment, resulting in shoreward transport of sediment across the shoreface (Daley and Cowell, 2012). Support for this interpretation is provided by the abundant sediment supply previously discussed, but also by the controlling influence of the aeolianite pinnacles, which not only dammed delta front deposits in their lee but also influenced the wave ravinement trajectory and resultant surface profile, over which the modern sediment unit was deposited. These results for the Xai-Xai coast also suggest that despite the absence of physiographic features such as reefs or rocky features outcropping on the shoreface seabed, which are often invoked for poor agreement with shoreface equilibrium profiles (e.g. Thieler et al., 1995; Kinsela et al., 2020), the occurrence of morphodynamic disequilibrium can be caused by shallow subsurface geological features and the trajectory of wave ravinement across the shoreface.

Overfit disequilibrium is associated with favourable conditions for onshore sediment transport from the lower shoreface, resulting in infilling of estuaries and generation of large sand dunes and ridges (Anthony and Aagaard, 2020). This is the case in the Xai-Xai coast, with the near complete infilling of the Limpopo tidal basin and development of extensive dune systems along the coast. At present, the extent of shoreface disequilibrium overfit indicated by the OA16 modelled profile implies that excess sediment in the lower shoreface in Xai-Xai is far from being exhausted. At multi-decadal timescales, the lower shoreface has the potential to continue to supply considerable amounts of sediment to the upper shoreface and beach, compensating the potential effects of rising sea levels and, consequently, maintaining shoreline stability or even contributing to accretion instead of retreat (Cooper et al., 2020).

It is prudent to remember that the profile models discussed above are purely two-dimensional and do not account for alongshore variability in morphology. In this instance, the extra morphological variations imposed by the SCRs may be a complicating factor. The localised overfit of the various profile models may thus be expected where SCRs are encountered (e.g. Hamon-Kerivel et al., 2020).

6. Conclusion

The shoreface stratigraphy of the Xai-Xai coast comprises 2 deltaic sequences overlying bedrock and separated by prominent aeolianite ridges. These units are truncated by the transgressive ravinement surface which shows a marked change in shore-normal gradient coincident with the underlying aeolianite pinnacles. The transgressive ravinement surface is overlain by ca.10 m of shoreface sediment and the modern seabed slope largely mirrors that of the ravinement surface. The modern shoreface comprises mobile sandy sediment and is fronted by a sequence of SCRs that point to sediment abundance.

The shoreface is influenced by multiple dynamic and geological variables, but no single model has conceptualised the influence of geological inheritance on the shoreface in addition to sea-level rise. At Xai-Xai the comparison of modelled equilibrium shoreface profiles against the observed profile suggest diverging morphodynamic shoreface disequilibrium states. On the basis of the thick sediment volume and shoreface-connected ridges, a sediment-abundant disequilibrium overfit is proposed for Xai-Xai. The shoreface's underlying stratigraphy points to additional geological controls on the geometry and trajectory of the shoreface evolution during and since the Holocene. In particular, submerged aeolianite ridges enhanced sediment retention/impoundment in the shelf, contributing to the deposition of abundant sediment supplied by the Limpopo River.

The morphodynamic state of the shoreface and the coupled coastal evolution of Xai-Xai indicate that areas characterised by disequilibrium overfit are likely to possess the shoreface sediment supply necessary to counteract SLR-induced shoreline erosion and ensure stability of sandy coastlines.

Supplementary data to this article can be found online at https://doi.org/10.1016/j.geomorph.2025.109884.

CRediT authorship contribution statement

A.N. Green: Writing – original draft, Supervision, Investigation, Funding acquisition, Formal analysis, Data curation, Conceptualization. **J.A.G. Cooper:** Writing – original draft. **H.L. Draycott:** Writing – original draft, Formal analysis. **C. Loureiro:** Writing – original draft, Formal analysis.

Declaration of competing interest

The authors declare that they have no known competing financial interests or personal relationships that could have appeared to influence the work reported in this paper.

Acknowledgements

We acknowledge Dr. Peter Ramsay for the geophysical and borehole data on which this study are based. We also acknowledge Bob De Decker and Alan Wijnberg of PRDW for the permission to access the jet probe data and multibeam data sets. We benefited from the helpful and thoughtful reviews by two anonymous reviewers, together with the inputs from the editor, Prof. D. Kennedy. HD acknowledges a scholarship from the National Research Foundation. CL acknowledges funding from FCT under contract CEECINST/00052/2021/CP2792/CT0011 (https://doi.org/10.54499/CEECINST/00052/2021/CP2792/CT0011) and projects LA/P/00069/2020 granted to the Associate Laboratory ARNET and UID/00350/2020 to CIMA-UALG.

Data availability statement

The data presented herein are available from the lead author on reasonable request. These data were part of a commercial project and are as such still of economic value and are not permitted to be uploaded freely.

References

Anthony, E.J., Aagaard, T., 2020. The lower shoreface: morphodynamics and sediment connectivity with the upper shoreface and beach. Earth Sci. Rev. 210, 103334.
Armitage, S.J., Botha, G.A., Duller, G., 2006. The formation and evolution of the barrier islands of Inhaca and Bazaruto, Mozambique. Geomorphology 82, 295–308.
Bateman, M.D., Holmes, P.J., Carr, A.S., Horton, B.P., Jaiswal, M.K., 2004. Aeolianite and barrier dune construction spanning the last two glacial–interglacial cycles from the southern Cape coast, South Africa. Quat. Sci. Rev. 23, 1681–1698.
Blott, S.J., Pye, K., 2001. GRADISTAT: a grain size distribution and statistics package for the analysis of unconsolidated sediments. Earth Surf. Process. Landf. 26 (11), 1237–1248.
Botha, G., Porat, N., 2007. Soil chronosequence development in dunes on the southeast African coastal plain, Maputaland, South Africa. Quat. Int. 162, 111–132.
Bowen, A.J., 1980. Simple models of nearshore sedimentation; beach profiles and longshore bars. In: McCann, S.B. (Ed.), The Coastline of Canada. Geological Survey of Canada, Paper vols. 80–10, 1–11. https://doi.org/10.4095/102213.
Cattaneo, A., Steel, R.J., 2003. Transgressive deposits: a review of their variability. Earth Sci. Rev. 62 (3–4), 187–228.
Chemane, D., Motta, H., Achimo, M., 1997. Vulnerability of coastal resources to climate changes in Mozambique: a call for integrated coastal zone management. Ocean Coast. Manag. 37 (1), 63–83.
Cooper, J.A.G., Green, A.N., 2023. Southern African sandy coasts in the context of near-future sea-level rise. Trans. R. Soc. S. Afr. 78 (3), 149–166.
Cooper, J.A.G., Pilkey, O.H., 2002. The Barrier Islands of Southern Mozambique. J. Coast. Res. SI36, 164–172. https://doi.org/10.2112/1551-5036-36.sp1.164.
Cooper, J.A.G., Pilkey, O.H., 2004. Sea-level rise and shoreline retreat: time to abandon the Bruun Rule. Glob. Planet. Chang. 43 (3–4), 157–171.

Cooper, J.A.G., Green, A.N., Loureiro, C., 2018. Geological constraints on mesoscale coastal barrier behaviour. Glob. Planet. Change 168, 15–34.
Cooper, J.A.G., Masselink, G., Coco, G., et al., 2020. Sandy beaches can survive sea-level rise. Nat. Clim. Chang. 10, 993–995. https://doi.org/10.1038/s41558-020-00934-2.
Cowell, P.J., Kinsela, M.A., 2018. Shoreface controls on barrier evolution and shoreline change. In: Barrier Dynamics and Response to Changing Climate. Springer, Cham, pp. 243–275.
Daley, M., Cowell, P.J., 2012. Long-term shoreface response to disequilibrium-stress: a conundrum for climate change. In: Proceedings of the 22nd NSW Coastal Conference. Macquarie, Port (16 pp).
De Lecea, A.M., Green, A.N., Strachan, K.L., Cooper, J.A.G., Wiles, E.A., 2017. Stepped Holocene sea-level rise and its influence on sedimentation in a large marine embayment: Maputo Bay, Mozambique. Estuar. Coast. Shelf Sci. 193, 25–36.
Dean, R.G., 1991. Equilibrium beach profiles: characteristics and applications. J. Coast. Res. 53–84.
Dyer, S.E., Green, A.N., Cooper, J.A.G., Hahn, A., Zabel, M., 2021. Response of a wave-dominated coastline and delta to antecedent conditioning and fluctuating rates of postglacial sea-level rise. Mar. Geol. 434, 106435.
Engelbrecht, L., Green, A.N., Cooper, J.A.G., Hahn, A., Zabel, M., Mackay, C.F., 2020. Construction and evolution of submerged deltaic bodies on the high energy SE African coastline: the interplay between relative sea level and antecedent controls. Mar. Geol. 424, 106170.
Engelbrecht, L.D., Green, A.N., Cooper, J.A.G., Mackay, C.F., 2022. Antecedent geological control on transgressive delta and shoreline preservation: examples from the SE African shelf. Mar. Geol. 454, 106934.
Fanti, V., Ferreira, Ó., Kümmerer, V., Loureiro, C., 2023. Improved estimates of extreme wave conditions in coastal areas from calibrated global reanalyses. Commun. Earth Environ. 4, 151.
Flemming, B.W., 1981. Factors controlling shelf sediment dispersal along the southeast African continental margin. Mar. Geol. 42 (1–4), 259–277.
Folk, R.L., Ward, W.C., 1957. Brazos River bar: a study in the significance of grain size parameters. J. Sediment. Petrol. 27, 3–26.
Green, A.N., Cooper, J.A.G., Salzmann, L., 2014. Geomorphic and stratigraphic signals of postglacial meltwater pulses on continental shelves. Geology 42 (2), 151–154.
Green, A.N., Ovechkina, M.N., Mostovski, M.B., 2012. Late Holocene shoreface evolution of the wave dominated Durban Bight, KwaZulu-Natal, South Africa: a mixed storm and current driven system. Cont. Shelf Res. 49, 56–64.
Hallermeier, R.J., 1981. A profile zonation for seasonal sand beaches from wave climate. Coast. Eng. 4, 253–277.
Hamon-Kerivel, K., Cooper, A., Jackson, D., Sedrati, M., Pintado, E.G., 2020. Shoreface mesoscale morphodynamics: a review. Earth Sci. Rev. 209, 103330.
Hamon-Kerivel, K., Jackson, D.W., Guisado-Pintado, E., Cooper, A., Sedrati, M., 2023. Spatial and temporal variability of shorefaces: a morpho-hydrodynamic controlled system. Estuar. Coast. Shelf Sci. 281, 108162.
Hapke, C.J., Lentz, E.E., Gayes, P.T., McCoy, C.A., Hehre, R., Schwab, W.C., Williams, S. J., 2010. A review of sediment budget imbalances along Fire Island, New York: can nearshore geologic framework and patterns of shoreline change explain the deficit? J. Coast. Res. 26 (3), 510–522.
Helland-Hansen, W., Martinsen, O.J., 1996. Shoreline trajectories and sequences; description of variable depositional-dip scenarios. J. Sediment. Res. 66 (4), 670–688.
Hersbach, H., Bell, B., Berrisford, P., et al., 2020. The ERA5 global reanalysis. Q. J. R. Meteorol. Soc. 146, 1999–2049. https://doi.org/10.1002/qj.3803.
Hoguane, A.M., Hill, A.E., Simpson, J.H., Bowers, D.G., 1999. Diurnal and tidal variation of temperature and salinity in the Ponta Rasa mangrove swamp, Mozambique. Estuar. Coast. Shelf Sci. 49 (2), 251–264.
Kinsela, M.A., Hanslow, D.J., Carvalho, R.C., Linklater, M., Ingleton, T.C., Morris, B.D., Allen, K.M., Sutherland, M.D., Woodroffe, C.D., 2020. Mapping the shoreface of coastal sediment compartments to improve shoreline change forecasts in New South Wales, Australia. Estuar. Coasts 45 (4), 1143–1169.
Kirkpatrick, L.H., Green, A.N., 2018. Antecedent geologic control on nearshore morphological development: the wave dominated, high sediment supply shoreface of southern Namibia. Mar. Geol. 403, 34–47.
Lamont, T., Roberts, M.J., Barlow, R.G., Morris, T., van den Berg, M.A., 2010. Circulation patterns in the Delagoa Bight, Mozambique, and the influence of deep ocean eddies. Afr. J. Mar. Sci. 32 (3), 553–562.
Lutjeharms, J.R., 2006. The Agulhas Current Retroflection. Springer Berlin Heidelberg.
Miguel, L.L.A.J., Castro, J.W.A., 2018. Aeolian dynamics of transgressive dunefields on the southern Mozambique coast. Africa. Earth Surf. Process. Landf. 43 (12), 2533–2546.
Miguel, L.L.A.J., Nehama, F.P.J., Castro, J.W.A., 2019. Lagoon-barrier system response to recent climate conditions and sea level rise, Mozambique, Africa. Estuar. Coast. Shelf Sci. 216, 71–86.
Milliman, J.D., Meade, R.H., 1983. World-wide delivery of river sediment to the oceans. J. Geol. 91 (1), 1–21.
Ortiz, A.C., Ashton, A.D., 2016. Exploring shoreface dynamics and a mechanistic explanation for a morphodynamic depth of closure. J. Geophys. Res. Earth 121 (2), 442–464.
Pilkey, O.H., Young, R.S., Riggs, S.R., Smith, A.S., Wu, H., Pilkey, W.D., 1993. The concept of shoreface profile of equilibrium: a critical review. J. Coast. Res. 33, 255–278.
Pretorius, L., Green, A.N., Cooper, J.A.G., 2016. Submerged shoreline preservation and ravinement during rapid postglacial sea-level rise and subsequent "slowstand". Geol. Soc. Am. Bull. 128 (7–8), 1059–1069.
Pretorius, L., Green, A.N., Cooper, J.A.G., 2018. Submerged beachrock preservation in the context of wave ravinement. Geo-Mar. Lett. 38, 19–32.
Preu, B., Spieß, V., Schwenk, T., Schneider, R., 2011. Evidence for current-controlled sedimentation along the southern Mozambique continental margin since Early Miocene times. Geo-Mar. Lett. 31, 427–435.
Richardson, A.G., 2005. The marine geology of the Durban Bight. Unpublished MSc Thesis, University of KwaZulu-Natal, Westville, p. 169.
Riggs, S.R., Cleary, W.J., Snyder, S.W., 1995. Influence of inherited geologic framework on barrier shoreface morphology and dynamics. Mar. Geol. 126 (1–4), 213–234.
Schüürman, J., Hahn, A., Zabel, M., 2019. In search of sediment deposits from the Limpopo (Delagoa Bight, southern Africa): deciphering the catchment provenance of coastal sediments. Sediment. Geol. 380, 94–104.
Schwab, W.C., Baldwin, W.E., Hapke, C.J., Lentz, E.E., Gayes, P.T., Denny, J.F., List, J.H., Warner, J.C., 2013. Geologic evidence for onshore sediment transport from the inner continental shelf: Fire Island, New York. J. Coast. Res. 29 (3), 526–544.
Schwartz, M.L., 1967. The Bruun theory of sea-level rise as a cause of shore erosion. J. Geol. 75 (1), 76–92.
Sete, C.I., Ruby, J., Dove, V., 2002. Seasonal Variation of Tides, Currents, Salinity and Temperature along the Coast of Mozambique. Instituto Nacional de Hidrografia e Navegacao, Maputo.
Soulsby, R.L., 1997. Dynamics of marine sands: a manual for practical applications. Oceanogr. Lit. Rev. 9 (44), 947.
Steel, R.J., Crabaugh, J., Schellpeper, M., Mellere, D., Plink-Björklund, P., Deibert, J., Loeseth, T., 2000. Deltas vs. rivers on the shelf edge: their relative contributions to the growth of shelf-margins and basin-floor fans (Barremian and Eocene, Spitsbergen). Deepwater Reserv. World 15 (1), 981–1009.
Thieler, E.R., Brill, A.L., Cleary, W.J., Hobbs, Gammisch, R.A., 1995. Geology of the Wrightsville Beach, North Carolina shoreface: Implications for the concept of shoreface profile of equilibrium. Mar. Geol. 126 (1–4), 271–287.
Wenau, S., Preu, B., Spiess, V., 2020. Geological development of the Limpopo Shelf (southern Mozambique) during the last sea level cycle. Geo-Mar. Lett. 40, 363–377.
Zecchin, M., 2007. The architectural variability of small-scale cycles in shelf and ramp clastic systems: the controlling factors. Earth Sci. Rev. 84 (1–2), 21–55.